Colloid & Polymer Science Colloid Polym Sci 272:903–909 (1994)

Small angle x-ray scattering study of ultra-high molecular weight poly(ethylene oxide) gamma irradiated in bulk

S. Tsvetkova and E. Nedkov

Institute of Polymers, Bulgarian Academy of Sciences, Sofia, Bulgaria

Abstract: The effect of gamma irradiation on the structure of ultra-high molecular weight poly(ethylene oxide) (UHMWPEO) has been investigated by small-angle x-ray scattering (SAXS). The pressed and irradiated polymer possesses quite strong diffuse scattering. That fact makes the direct determination of the main structural parameters very difficult. To solve the problem a modification of the standard evaluating methods is suggested. Thus, the separation of the porous scattering from that of structural formations of PEO becomes possible. The application of a collimation correction according to Schmidt's method enables to separate diffuse and discrete parts in the scattering. Dependences of the long period, the gyration radii, and the difference between densities of crystalline and amorphous phases on the irradiation dose show that the irradiation increases the density of amorphous areas. A packing of the lamellar aggregates and increase of the porous sizes are observed.

Key words: Small angle x-ray scattering – collimation correction – Guinier approximation – Porod's invariant – ultra-high molecular weight poly(ethylene oxide)

Introduction

Small-angle x-ray scattering (SAXS) investigations of poly(ethylene oxide) (PEO) have been carried out many times. The object of such studies has mainly been low molecular weight fractions of the polymer [1–3]. Determination of the long period of PEO have been the aim of these works. It is established that the value of the long period depends on molecular weight and crystallization temperature. There are dynamical analyses of isothermal crystallization of low molecular weight fractions made by SAXS [4].

The long period of PEO with molecular weight of about a hundred thousand is approximately 180 Å. A faint discrete reflex is observable on a strong diffuse scattering background [2].

All our efforts to find reports in the literature about SAXS determination of long period of ultra-high molecular weight PEO (UHMWPEO) did not yield any. A probable cause is the quite powerful diffuse scattering of PEO in comparison with other polymers. An example is the comparison with poly(propylene oxide) PPO (Fig. 1), even under low molecular weights [5]. Another probable cause is the formation of numerous micropores with sizes in the order of angstroms in the structure of ultra-high molecular weight polymers. Pressed and sintered ultra-high molecular weight polyethylene (UHMWPE) does not display any long period because of the presence of micropores [6]. The investigations of blends of UHMWPE and isotactic polypropylene (i–PP) establish that increasing PE contents leads to increasing intensity of diffuse scattering and gradual disappearing of discrete reflex [7]. Our earlier attempts to obtain discrete scattering from UHMWPEO were also unsuccessful.

The aim of the present work is to report the effect of gamma irradiation on the structure of UHMWPEO. An attempt to separate discrete scattering from diffuse scattering is made. Some

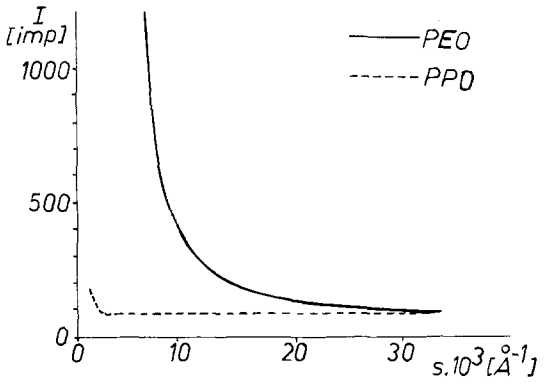

Fig. 1. Comparison between SAXS of PEO and PPO (using data of Gomza, Shilov, Lipatov [5]).

structural parameters of UHMWPEO are calculated from the measured data.

Materials and Methods

SAXS experiments are carried out by diffractometer KRM-1 (USSR) using Ni filtered CuK_α radiation with slit collimated incident beam. A scintillation counter and single channel analyzer are used to detect the reflected beam. A scheme of the apparatus is shown in Fig. 1. The intensity is obtained in counts per second and recalculated in arbitrary units versus variable:

$$s = (4\pi \sin\vartheta/\lambda) \cdot 10^3/\text{Å}^{-1} = (4\pi \sin\vartheta/\lambda) \cdot 10^4/\text{nm}^{-1}\,, \quad (1)$$

where 2ϑ is the scattering angle and λ is the wave length ($\lambda = 1.54$ Å). SAXS curves are obtained in the range:

$$4 \leq s \cdot 10^3/\text{Å}^{-1} \leq 40 \quad \text{(corresponding to } 4' \leq 2\vartheta \leq 40') \quad (2)$$

with step $\Delta s = 0.1 \cdot 10^3/\text{Å}^{-1}$ and a maximum rate of 1000 counts per second.

Collimation correction according to Schmidt's method [8–10] and approximation according to the law of Guinier [11] are performed on the experimental data. A long period, gyration radius, and Porod's invariant [12, 13] are determined. The difference between crystalline and amorphous densities is determined from Porod's invariant under the formula:

$$Q = k\alpha(1-\alpha)(\rho_c - \rho_\alpha)^2\,, \quad (4)$$

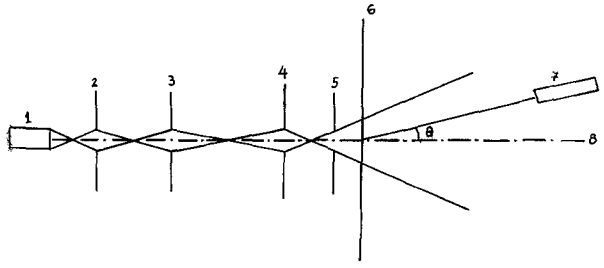

Fig. 2. Scheme of the apparatus KRM-1: 1 – x-ray source; 2, 3, 4, 5 – collimation slits; 6 – sample plane: 7 – scintillation detector; 8 – primary beam direction.

where Q is the invariant of Porod:

$$Q = UT \int_0^\infty I(s)\mathrm{d}s\,, \quad (5)$$

and k is the calibration factor, α the degree of crystallinity, ρ_c the density of crystalline areas, and ρ_α is amorphous density. In this case the integration in the numerator may only involve the radial component of the scattering vector s. Being a function of the scattering angle only, it is a one-dimensional value. We have assumed that $(\rho_c - \rho_\alpha)$ for the unirradiated PEO is known from other studies [14] and, furthermore, have used values of α determined by WAXS [15]. Calibration factor k for this series of samples is calculated from the value of Q for the unirradiated sample. Furthermore, the thickness of the lamella H was calculated by the formula:

$$H = \alpha L\,, \quad (6)$$

where α is the degree of crystallinity and L is the mean distance between lamellae (long period).

Results

The data obtained initially are shown in Fig. 3. The initial intensities are marked as I_{beg}. A very slight, discrete shoulder is noticeable against a power diffuse scattering background. We assumed that the discrete scattering is a single maximum in the narrow angle range. Dividing of the discrete maximum from the diffuse scattering was made in the following procedure:

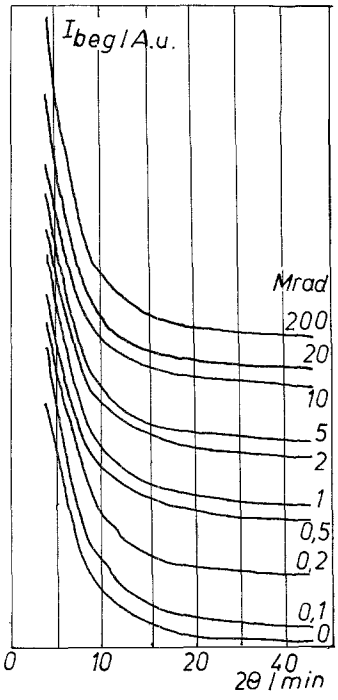

Fig. 3. SAXS patterns obtained by a slit collimation diffractometer.

Diffuse scattering can be described by law of Guinier:

$$I_{\text{diff}}(s) = I(0)\exp(-R_g^2 s^2/3)\,, \tag{7}$$

where $I(0)$ is the zero intensity (constant corresponding to the approximated intensity at $s = 0$) and R_g is the gyration radius. The curve $\ln I_{\text{diff}}$ versus s^2 must be linear. But this dependence was fitted well by two straight lines in the range outside the presumable maximum. Two gyration radii were calculated from the slopes of these straight lines (RG01, RG02). The integral diffuse intensity is calculated in the whole angle range under the two lines. It is subtracted from the experimental one (I_{beg}). In this way the intensity of discrete scattering was obtained. The location of the presumed maximum of discrete scattering was calculated by averaging the angle range where the discrete scattering was considerably differing from zero/16/:

$$S_m = \int_0^\infty s I_{\text{discr}}(s)\mathrm{d}s \Big/ \int_0^\infty I_{\text{discr}}(s)\mathrm{d}s\,. \tag{8}$$

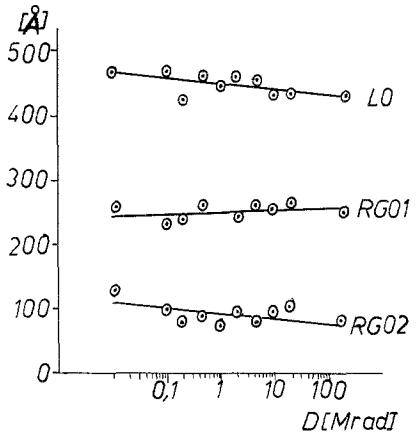

Fig. 4. Long period L0 and gyration radii RG01, RG02 calculated from the curves shown in Fig. 3.

The long period L0 and two gyration radii RG01 and RG02 obtained in the above manner from the investigated doses are shown in Fig. 4. In the following, under L0, RG01, RG02, etc. their dependencies on the irradiation dose shall be understood.

The similar curves $\ln I_{\text{diff}}$ versus s^2 for gamma irradiated PP [16] are linear. In this case the application of the above method [16] leads to results which are in agreement with conclusions of Keller, Ungar, and Grabb about concentrating the radiation defects on the lamellar surface [17]. In our case, the groundlessness of the assumption for a single maximum in a narrow angle range and the intangible physical meaning of the two gyration radii lead us to leave this way of evaluating the experimental data and to find another way for processing.

In the beginning, collimation correction was applied according to the method of Schmidt [10]. The intensities reduced to pin-hole source (I_{corr}, Fig. 5) are quite different from the initially obtained (I_{beg}, Fig. 6). Two discrete reflexes are outlined against the diffuse scattering. The long periods L1 and L2 calculated from the location of the reflexes are shown in Fig. 7. They are compared with L0 which was obtained from uncorrected data. The attempt to apply Guinier's law shows that the curves $\ln I_{\text{diff}}$ versus s^2 (Fig. 8) may be well approximated by three straight lines in the ranges:

$$4 \le s\cdot 10^3/\text{Å}^{-1} \le 10,\quad 10 \le s\cdot 10^3/\text{Å}^{-1} \le 24$$
$$\text{and } 24 \le s\cdot 10^3/\text{Å}^{-1} \le 40\,.$$

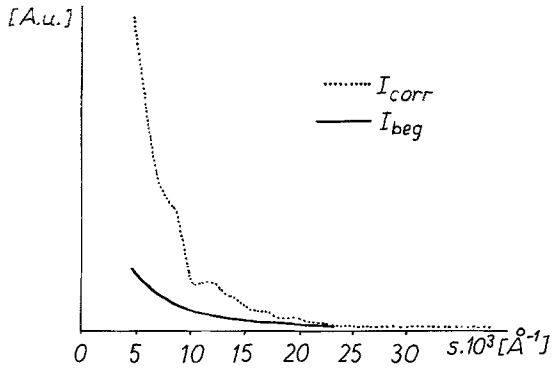

Fig. 5. Comparison between intensities of SAXS before and after collimation correction: I_{beg} – before correction, I_{corr} – after correction.

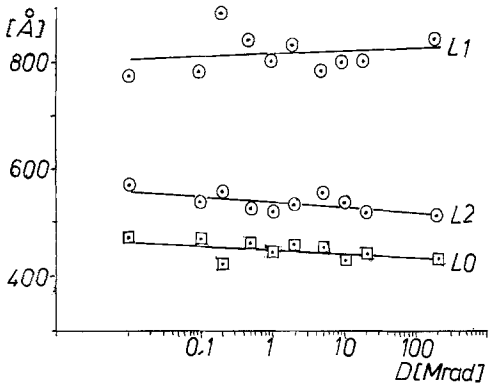

Fig. 7. Long periods L1 and L2 calculated from locations of discrete reflexes in the corrected intensities in comparison with those calculated from uncorrected intensities long period L0.

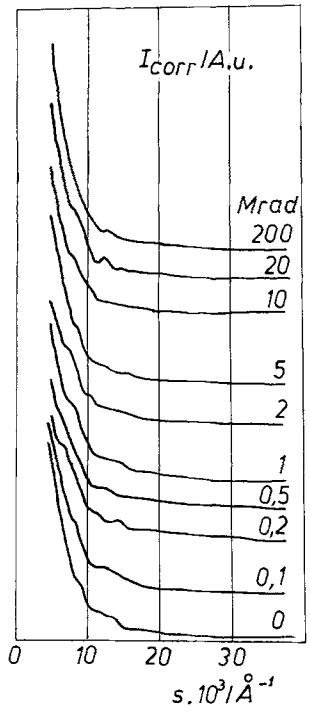

Fig. 6. Reduced to pin-hole collimated incident beam intensities of SAXS.

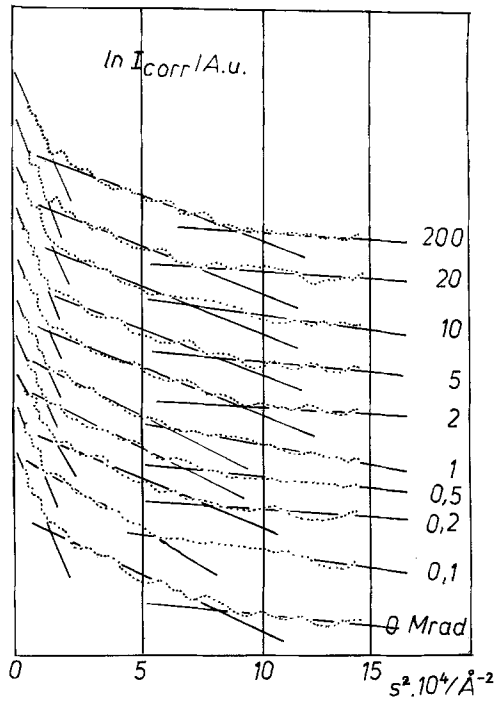

Fig. 8. Guinier plots calculated from corrected intensities for investigated doses.

The three gyration radii calculated from the slopes of the straight lines are shown in Fig. 9. The dependencies of the corresponding three ranges of radii on the irradiation dose are marked as RG1, RG2, and RG3. I1(0), I2(0) and I3(0) are the zero intensities calculated by approximation $s = 0$. Their dependencies on irradiation dose are shown in Fig. 10.

L1, RG1, and I1(0) are dispersed in a wide range of values and increase poorly with dose (Figs. 7, 9, 10). L2, RG2, and I2(0) give values which regularly decrease with irradiation dose (Figs. 7, 9, 10). The values of L2 are near those of L0 calculated from uncorrected data (Fig. 7). The

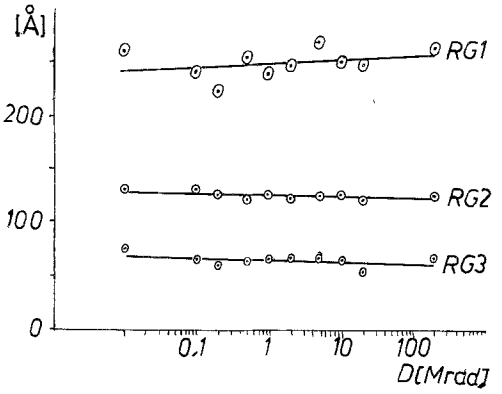

Fig. 9. Dependencies of the gyration radii RG1, RG2, RG3 calculated from the Guinier curves on the irradiation dose.

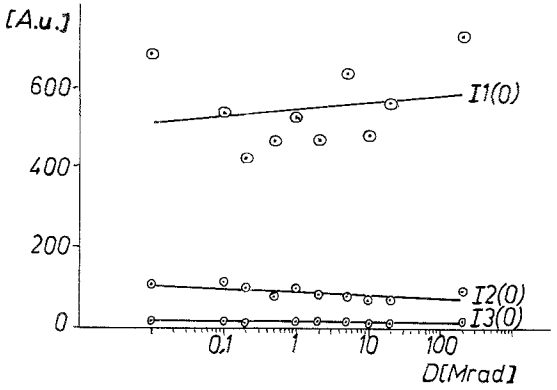

Fig. 10. Zero intensities of SAXS calculated by Guinier approximation as a function of the irradiation dose.

values of RG1 (Fig. 7) are near those of RG01 (Fig. 4). The values of RG02 (Fig. 4) are larger than those of RG3 and smaller than those of RG2 (Fig. 9). On the basis of the above comparison, we assume that the scattering in the area $10 \leq s \cdot 10^3/\text{Å}^{-1} \leq 24$ is due to structural formations of the polymer. The scattering in the area $4 \leq s \cdot 10^3/\text{Å}^{-1} \leq 10$ is due to the presence of pores in the bulk of the polymer. The quite small values of I3(0) in comparison with I1(0) and I2(0) (Fig. 10) enable to divide the scattering in the area $24 \leq s \cdot 10^3/\text{Å}^{-1} \leq 40$ as a background. The assumptions made are in good agreement with our observations on the morphology of the UHMWPEO [15]. Assuming the above statements, it has been presumed that the scattering in the range $4 \leq s \cdot 10^3/\text{Å}^{-1} \leq 10$ could be described as caused

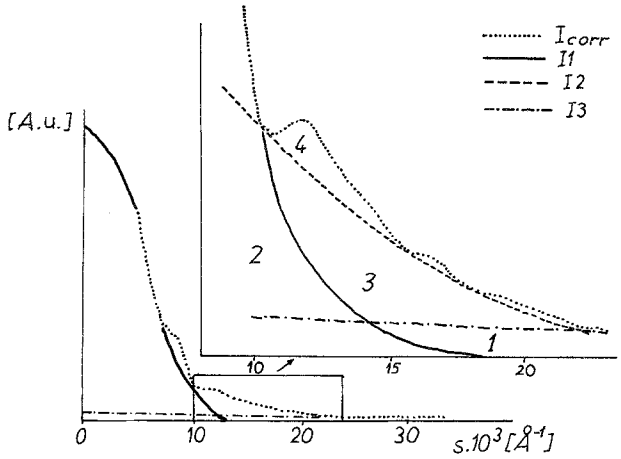

Fig. 11. Extracting of the background scattering and the porous scattering from corrected intensity. Guinier approximation to divide discrete polymer scattering from the diffuse one: 1 – background; 2 – porous scattering; 3 – diffuse polymer scattering; 4 – discrete polymer scattering.

by the two-phase system formed by polymer and pores. On the other hand, discussing the scattering in the range $10 \leq s \cdot 10^3/\text{Å}^{-1} \leq 24$, the system could be considered as another type of two-phase one, formed by crystalline and amorphous polymer.

The intensities I1 and I3 restored under the whole investigated range obtained by fitting in the ranges $4 \leq s \cdot 10^3/\text{Å}^{-1} \leq 10$ and $24 \leq s \cdot 10^3/\text{Å}^{-1} \leq 40$, respectively, are shown in Fig. 11. In the same figure is also shown corrected intensity (I_{corr}). The structural parameters of PEO were determined after elimination of the background scattering and the porous scattering. The thus obtained intensity I_{PEO} includes diffuse (I_{diff}) and discrete (I_{discr}) scattering due to the polymer:

$$I_{corr} - \text{MAX}(I1, I3) = I_{PEO} = I_{diff} + I_{discr}. \quad (10)$$

A new Guinier approximation of ln I_{corr} vs s^2 in the range $10 \leq s \cdot 10^3/\text{Å}^{-1} \leq 24$ by the smallest value points was made to separate I_{diff} from I_{discr}. It is also shown in Fig. 11. Lorenz corrected intensities I_{PEO}, I_{diff}, and I_{discr} for different doses are shown in Fig. 12. Dependencies of the calculated integral surfaces of diffuse and discrete scattering:

$$P_{diff} = \int_0^\infty I_{diff}(s)ds \qquad P_{discr} = \int_0^\infty I_{discr}(s)ds \quad (11)$$

are shown in Fig. 13.

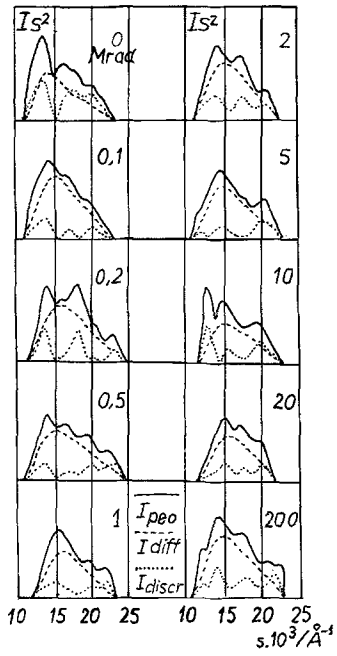

Fig. 12. SAXS from PEO after separating of the discrete part from the diffuse part and Lorenz correction: I_{PEO} – summary scattering due to structural formations of PEO, I_{discr} – discrete polymer scattering, I_{diff} – diffuse polymer scattering.

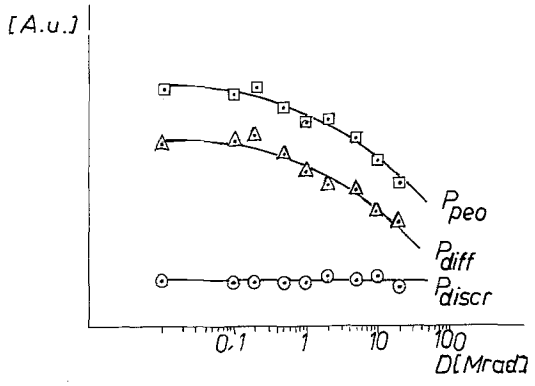

Fig. 13. Dependencies of the integral scattering surfaces of diffuse and discrete scattering on the irradiation dose.

Discussion

Ultra-high molecular weight PEO possesses lamellar structure as typical for many polymers. Bulk pores are observed as a further characteristic of ultra-high molecular weight polymers. These facts enable the consideration of PEO as a three-phase system. Its components are: lamellar stacks, amorphous layers outside the stacks, and micropores.

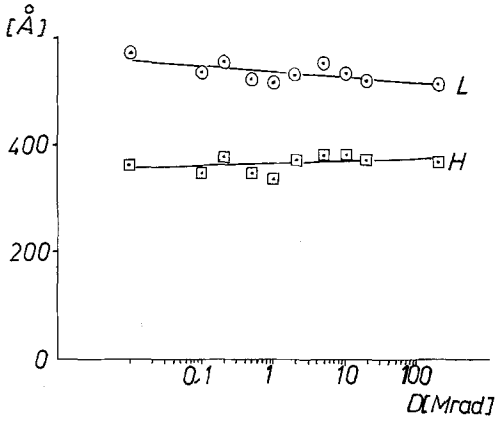

Fig. 14. Dependence of the long period (L) and the lamellar thickness (H = αL) on the irradiation dose.

The interaction of gamma quantum with polymer molecules very often causes breaking of the chains and creation of free radicals. Free radicals obtained may react in the following ways:

If they are in amorphous regions the flexibility of the PEO molecules allows easy deactivation, after which such radiation defects as double bonds, chain branchings or free ends remain in the amorphous areas. If the free radicals are in the crystalline regions the fast recombination is most probable because of the low mobility of the molecules. The recombination is attended by emission of energy surplus as an exiton into the crystal [18, 19]. We assume that the motion of the exiton is most probably along the chains to the lamellar surface. It has been caught by different types of dislocations and radiation defects on the lamellar surface have been made. There is also probable migration of the free radicals along the chains as far as the lamellar surface where they have been deactivated easily.

The processes described above lead to pushing radiation defects off the crystalline regions into amorphous ones as the thickness of the lamella has not been changed (H, Fig. 14). At the same time, the decreasing of the long period (L, Fig. 14) points to the fact that the amorphous surface layers of the lamellae become thinner and denser. Also, with increasing of the dose the difference between crystalline density and the amorphous one decreases (Fig. 15). Generally, the volume of

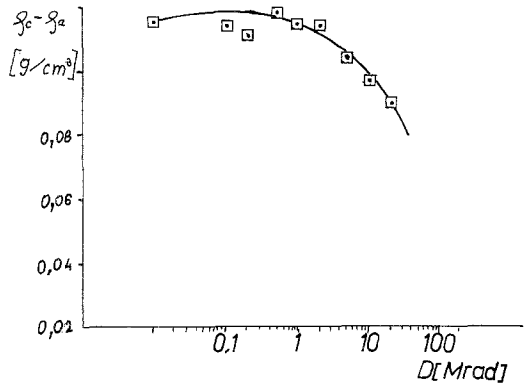

Fig. 15. Dependence of the difference between crystalline and amorphous densities on the irradiation dose.

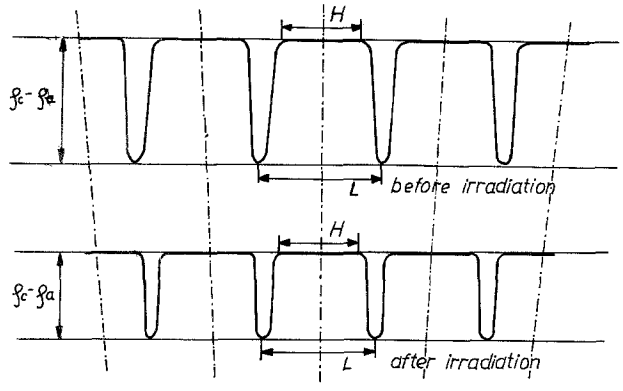

Fig. 16. Scheme of changes in the lamellar structure of PEO after irradiation: L – long period (mean distance between lamellae), H – thickness of the crystalline lamella, ρ_c – density of the crystalline phase, ρ_a – density of the amorphous phase.

the lamellar aggregates decreases. The changes described above are shown schematically on Fig. 16. Since changes of macro volume are not observed this may be possible only when the size of existing pores increases. This conforms well to dependencies of L1 (Fig. 6) and RG1 (Fig. 8) on the irradiation dose. Yet, both parameters attributed to pores show slight increasing with dose. They lead to two other effects: unclearing of the lamellar boundaries and congestion of the amorphous regions.

Conclusions

The irradiation of UHMWPEO with gamma rays in the bulk mainly induces changes in the amorphous regions. These reflect the decrease of the difference between crystalline and amorphous density. The congestion of the lamellar aggregates described above causes increasing of the porous volume in the bulk of the polymer.

References

1. Price FP, Kilb RW (1962) J Polym Sci 57:395.
2. Balta Calleja FJ, Keller A (1964) J Polym Sci A2:2171
3. Arlie JP, Spegt P, Skoulios A (1967) Die Makromolekulare Chemie 104:212
4. Cheng SZD, Zhang A, Chen J (1990) J Polym Sci C28:233
5. Gomza J, Shilov V, Lipatov Y (1982) Die Angewandte Makromolekulare Chemie 103:1
6. Unpublished data
7. Nedkov E, Atanasov A (1985) Bulg J Phys 12:401
8. Taylor TR, Schmidt PW (1967) Acta Physica Austriaca 25:294
9. Schmidt PW, Fedorov BA (1978) J Appl Cryst 11:411
10. Schmidt P, Walter G (1981) J Appl Cryst 14:28
11. Alexander LE (1969) X-Ray Diffraction Methods in Polymer Science 298, J. Willey – Interscience, New York
12. Alexander LE (1969) X-Ray Diffraction Methods in Polymer Science 291, J. Willey – Interscience, New York
13. Svergun DI, Feigin LA (1986) X-Ray and Neutron Small Angle Scattering 167, Science, Moscow
14. Wunderlich B (1976) Macromolecular Physics, Vol. 1, 447, Ed. Mir, Moscow
15. Nedkov E, Tsvetkova S, Radiat Phys Chem (in press).
16. Krestev V, Velikov V, Nedkov E (1989) National Simposium "X-Ray Diffraction Methods", Nesebar, Bulgaria
17. Keller A, Ungar G, Grabb DT (1983) Radiat Phys Chem 22:849
18. Dole M (1978) The Radiation Chemistry of Macromolecules, Academic Press, Moscow
19. Ranby B, Rabek JF (1978) Photodegradation, Photostabilisation, Photooxydation of Polymers, Mir, Moscow

Received February 9, 1993;
accepted November 29, 1993

Authors' address:

Dr. E. Nedkov
Institute of Polymers
Bulgarian Academy of Sciences
1113 Sofia, Bulgaria